Morphological transition between diffusion-limited and ballistic aggregation growth patterns

S. C. Ferreira, Jr.*
Departamento de Física, Universidade Federal Viçosa, 36571-000, Viçosa, Minas Gerais, Brazil

S. G. Alves, A. Faissal Brito, and J. G. Moreira
Departamento de Física, Universidade Federal de Minas Gerais, Caixa Postale 702, 30161-970, Belo Horizonte, Minas Gerais, Brazil
(Received 9 November 2004; revised manuscript received 3 March 2005; published 16 May 2005)

In this work, the transition between diffusion-limited (DLA) and ballistic aggregation (BA) models was reconsidered using a model in which biased random walks simulate the particle trajectories. The bias is controlled by a parameter λ, which assumes the value $\lambda=0$ (1) for the ballistic (diffusion-limited) aggregation model. Patterns growing from a single seed were considered. In order to simulate large clusters, an efficient algorithm was developed. For $\lambda\neq 0$, the patterns are fractal on small length scales, but homogeneous on large ones. We evaluated the mean density of particles $\overline{\rho}$ in the region defined by a circle of radius r centered at the initial seed. As a function of r, $\overline{\rho}$ reaches the asymptotic value $\rho_0(\lambda)$ following a power law $\overline{\rho}=\rho_0+Ar^{-\gamma}$ with a universal exponent $\gamma=0.46(2)$, independent of λ. The asymptotic value has the behavior $\rho_0\sim|1-\lambda|^{\beta}$, where $\beta=0.26(1)$. The characteristic crossover length that determines the transition from DLA- to BA-like scaling regimes is given by $\xi\sim|1-\lambda|^{-\nu}$, where $\nu=0.61(1)$, while the cluster mass at the crossover follows a power law $M_{\xi}\sim|1-\lambda|^{-\alpha}$, where $\alpha=0.97(2)$. We deduce the scaling relations $\beta=\nu\gamma$ and $\beta=2\nu-\alpha$ between these exponents.

DOI: 10.1103/PhysRevE.71.051402 PACS number(s): 61.43.Hv, 05.40.Fb, 47.53.+n, 47.54.+r

I. INTRODUCTION

The pattern formation in nonequilibrium processes is a longstanding problem in statistical physics [1–3]. In particular, the diffusion-limited aggregation (DLA) model [4] is a noteworthy example in which a very simple algorithm generates disorderly fractal clusters. This model was related to several physical and biological applications, such as electrodeposition [5], viscous fingering [6], bacterial colonies [7], and neurite formation [8]. In the DLA model, particles released at a point distant from the cluster execute random walks until they find a neighbor site of the cluster and irreversibly stick at this site. If the random walks are replaced by ballistic trajectories at random directions, we have the ballistic aggregation (BA) model [9]. In contrast to DLA, the BA model generates disordered nonfractal clusters with nontrivial scaling properties [2,10].

Due to its importance as a fundamental model, several generalizations of the DLA model were proposed [1,2]. In particular, those models in which the particle trajectories are biased random walks were investigated [11–16]. In these models, on short length scales the particle trajectories are common random walks with fractal dimension 2.0, whereas on longer length scales the bias becomes dominant and the dimensionality of the walk is 1.0. Clusters grown using this type of walk must behave like the DLA model on short length scales, while nonfractal patterns are observed on longer ones. Consequently, the mass of a cluster of size l is given by

$$M(l) = l^{d_f} f(l/\xi), \tag{1}$$

in which

$$f(x) \sim \begin{cases} \text{const} & \text{if } x \ll 1, \\ x^{d-d_f} & \text{if } x \gg 1. \end{cases} \tag{2}$$

Here, d is the space dimension, d_f is the DLA fractal dimension, and ξ is the crossover radius from DLA- to BA-like scaling regimes. This idea was first considered by Meakin [11]. In his model, the simulations start with a single seed at the center of a square lattice and the drift of all trajectories is in a fixed lattice direction. Along the walk, the particle is moved one lattice unit in the drift direction with probability P, or moves to one of its four next-neighbor sites with probability $1-P$. The model generates patterns with a growth tendency in the opposite direction of the drift. The author argues that the crossover from the DLA-like structure on short length scales to a compact structure on longer ones is characterized by a length $\xi\sim P^{-1}$. However, using a renormalization group approach, Nagatani found $\xi\sim P^{-1/(d-d_f)}$ [17]. Kim *et al.* [12,13] studied lattice models with a global drift to the seed, in which the particles have a higher probability to move to the nearest neighbor representing the shortest distance away from the seed. The pattern morphologies are ruled by the lattice anisotropy and their fractal dimension is 1. Nagatani [14] considered the effects of positive and negative radial drifts in the DLA model. In the positive case the cluster fractal dimension is asymptotically 2, while eccentric patterns with dimension 1 were found for the negative case. Other models [15,16] consist of deposition processes on a d-dimensional substrate in which the walk drift is in the substrate direction.

In the present paper, we are interested in the transition from DLA to BA models when the random or ballistic trajectories of DLA and BA models, respectively, are replaced by biased random walks with a random drift direction. The central concern of this work is the fact that all real fractals

*Electronic address: silviojr@ufv.br

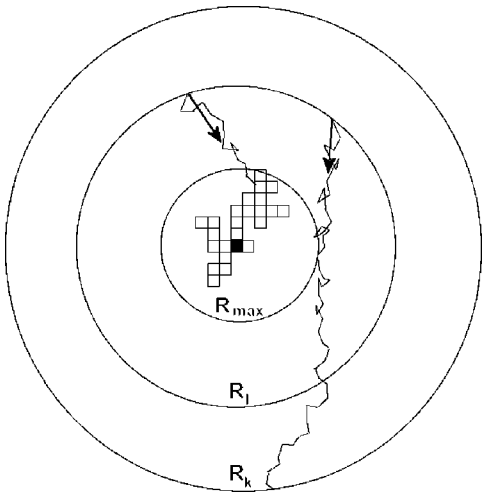

FIG. 1. Schematic representation of the model.

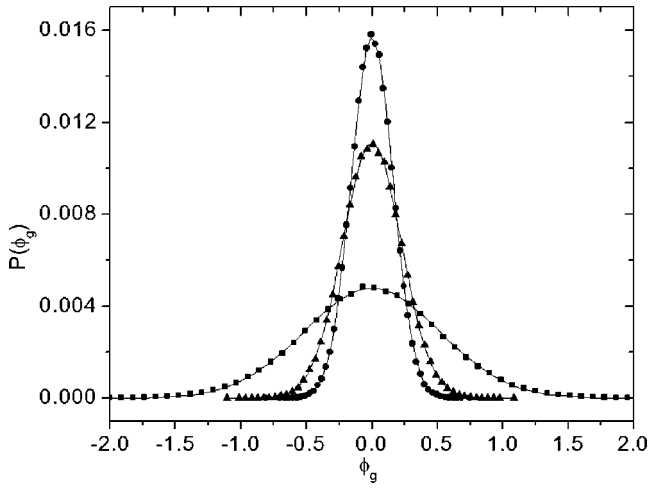

FIG. 2. Angle distributions for biased random walkers with preferential direction $\varphi=0$ and the correspondent Gaussian fits. The curves correspond to $\lambda=0.99$ and $R_s=200$ (squares), $\lambda=0.99$ and $R_s=1000$ (triangles), and $\lambda=0.90$ and $R_s=200$ (circles). Other parameter sets used in the simulations provide fits better than those shown in this figure. For all couples λ and R_s used in the simulations a correlation coefficient $r^2 \geqslant 0.999$ was required.

exhibit scaling only on limited ranges and, consequently, a quantitative analysis of both experiments and simulations demands a deep understanding of these crossovers. The outline of the paper is the following. In Sec. II, the model and the respective computational algorithm are described. In Sec. III, the simulational results are presented and discussed. Finally, some conclusions are drawn in Sec. IV.

II. MODELS AND METHODS

As in the original DLA and BA models, at the beginning of the simulations a unique seed localized in the center of the lattice constitutes the cluster. Then, particles are sequentially released on a circle distant from the cluster and execute biased random walks. The distance between the center of the lattice and the launching circle is denoted by R_l. The biased walks are defined by

$$x_{n+1} = x_n + \cos(\varphi + \lambda\theta_n),$$

$$y_{n+1} = y_n + \sin(\varphi + \lambda\theta_n), \tag{3}$$

where x_n and y_n are the particle coordinates at the nth step of the walk, φ is a random angle that defines the bias direction, $\lambda \in [0,1]$ is the parameter that controls the random component of the trajectories, and θ_n is a random direction. The variables φ and θ_n are in the range $[-\pi,\pi]$. Notice that φ is defined at the beginning of the walks, whereas θ_n assumes random values for each walk step. One can see that the particular cases $\lambda=0$ and 1 recover the BA and DLA models, respectively. If the particle visits a site neighboring the cluster it irreversibly joins this site. However, if the distance between the particle and the cluster is too large, i.e., larger than a killing radius R_k, the particle is excluded and a new one is released at the launching circle. In order to determine when a walker is neighboring a cluster site, its lattice position was defined as the next integer value of its real coordinates defined by Eq. (3). The majority of the results presented in this work refer to the square lattice version of the model.

The previously introduced variables (R_l and R_k) must be as large as possible. However, computational limitations restrict the use of R_l and R_k values. We defined $R_l=R_{\max}+R_0$, where $R_{\max}$ is the maximum distance from the center of the lattice of a particle belonging to the cluster. For DLA and BA models R_0 can be of the order of some lattice units [1,2]. However, for the model with biased random walks the pattern morphologies are strongly dependent on this value. Our tests suggest that the patterns become insensitive to R_0 variations when $R_0>300$, in agreement with the values adopted by Kim [16] for a model of deposition of biased random walks on a substrate. Thus, $R_0=400$ was used in all simulations. The killing radius R_k must be 10 to 100 times $R_{\max}$ for very large DLA clusters [1] whereas an R_k only some lattice units larger than $R_{\max}$ is necessary for the BA model. Due to the bias present in the random walks, we used the same strategy adopted by Kim [16], i.e., $R_k=2R_{\max}+R_0$. Figure 1 illustrates two tentatives, one successful and the other frustrated, to add a new particle to the cluster.

To analyze the transition between BA and DLA it is necessary to simulate large clusters using lattices containing up to $10^4\times10^4$ sites, especially when $\lambda \lesssim 1$. Consequently, the computational time becomes prohibitive and an efficient algorithm is necessary. A technique commonly used to simulate large DLA and related models is to allow the particles to execute long steps in random directions if they are far from the cluster [18–21]. This procedure is correct because the probability that a random walker crosses the circle centered on its initial position in a given angle ϕ is uniformly distributed in the interval $[-\pi,\pi]$. However, for the biased random walkers this is not true. Indeed, the probability density distributions are concentrated around the direction φ. For λ not very close to unity or for large steps, the probability distributions are very well fitted by Gaussian curves centered at φ, as illustrated in Fig. 2. Using this fact, the following proce-

TABLE I. σ values determined with the Gaussian least squares fits.

λ	$\sigma(R_s=200)$	$\sigma(R_s=1000)$
0.100	0.02585	0.01202
0.300	0.07591	0.03413
0.500	0.12535	0.05613
0.700	0.18206	0.08139
0.900	0.31933	0.14216
0.950	0.45109	0.20057
0.990	1.03575	0.45130
0.995	1.53278	0.63451

dure was adopted. If the distance between the random walker and the cluster is larger than a value $R_s+\delta$, it executes a jump of length R_s. Thus, a long jump cannot lead the walker a distance smaller than δ. The jump direction is $\phi=\varphi+\phi_g$, where ϕ_g is a random number between $-\pi$ and π selected from a Gaussian distribution

$$P(\phi_g)=\frac{1}{\sigma\sqrt{\pi/2}}\exp\left(-2\frac{\phi_g^2}{\sigma^2}\right). \tag{4}$$

In order to obtain the Gaussian width σ for each couple λ and R_s, a large number of biased random walks (10^6-10^7) were simulated and a histogram of the probabilities built (Fig. 2). Then the σ value can be determined using least squares Gaussian fits. The quality of fits is improved as larger R_s values and smaller λ values are used. Therefore, the R_s values should be sufficiently large to reproduce good fits, in particular for $\lambda \lesssim 1$. Furthermore, several R_s values can be used in the same simulation improving the algorithm efficacy. We used two values: $R_s=200$ and 1000. The σ values used in the simulations are shown in Table I. Also, $\delta=20$ was used. All tests show that the growth patterns are not sensitive to the δ value. It is worth noting that the Gaussian distribution is not normalized in the interval $[-\pi,\pi]$ and, obviously, this is not the actual angle distribution for the present problem. However, the very good fits to the angle distributions justify the use of the Gaussian functions.

III. RESULTS AND DISCUSSION

The first stage of the present work was to confirm the validity of the previous defined algorithm. We simulate relatively small lattices containing $10^3\times10^3$ sites with and without the optimization for $\lambda=0.99$. In Fig. 3, comparisons between clusters generated with (top) and without (bottom) the optimization are shown. Comparing the patterns, one can see that they are statistically indistinguishable. Using the mass-ratio method, the fractal dimensions of the patterns generated with and without the algorithm were $d_f=1.70\pm0.02$ and 1.72 ± 0.02, respectively, and the exponents of the radius of gyration, defined by $r_g\sim n^{\zeta}$ (n is the number of cluster particles) [2], were $\zeta=0.560\pm0.003$ and 0.561 ± 0.002, respectively. These exponents reinforce the algorithm validity. Concerning the computational time, a single run to generate one

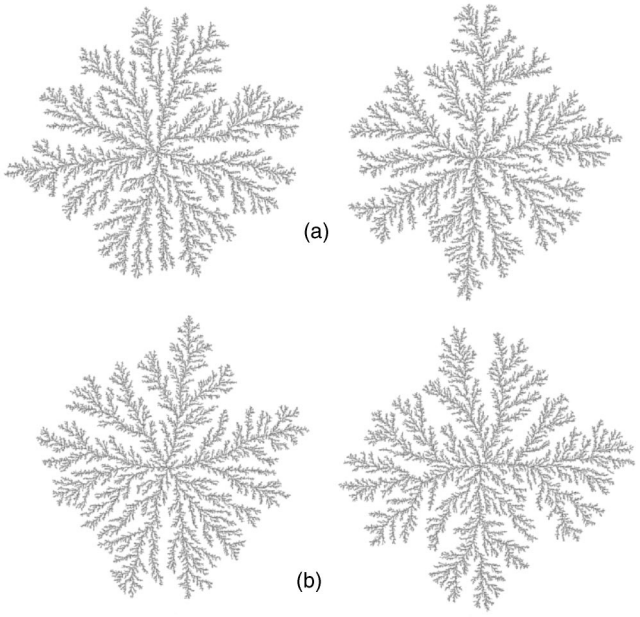

FIG. 3. Two clusters generated (a) using or (b) not using the optimization. In these simulations, lattices of size $L=1000$ and $\lambda=0.99$ were used.

of the clusters shown in Fig. 3 without the optimization takes about 1 h in a 3 GHz pentium IV, but the same simulation is done in 10 min using the optimization. Therefore, even for small lattices the simulation performance is greatly improved when our optimized algorithm is used.

Figure 4 shows growth patterns for distinct λ values. These patterns were generated with the optimization at lattices containing $10^3\times10^3$ sites. The simulations stopped when the aggregate reaches the lattice edge. A continuous transition from disordered and dense to ramified clusters is observed. For small λ values the patterns are essentially BA-like but the patterns become very similar to the DLA clusters as $\lambda\to1$. Indeed, the cluster generated with $\lambda=0.995$ is characterized by the square lattice anisotropy, a signature of the DLA model [1,2]. However, one expects that all patterns become asymptotically homogeneous with a finite characteristic size for the empty regions.

In order to quantify the DLA to BA morphology transition, the mean particle density in the inner regions of the cluster was evaluated. This mean density $\overline{\rho}(r)$ is defined as the ratio between the number of occupied sites and the total number of sites in a region delimited by a circle of radius r centered at the initial seed. Since one expects asymptotically nonfractal clusters, the density must reach a finite value ρ_0 as $r\to\infty$. Nevertheless, the approach to the constant density is very slow and takes a scale invariant form

$$\overline{\rho}(r)=\rho_0+Ar^{-\gamma}. \tag{5}$$

Here, γ is a correction to the fractal dimension and A a constant. This scaling hypothesis was also used by Liang and Kadanoff [10] to study the driven ballistic aggregation, in which the particles trajectories are in a single direction. They

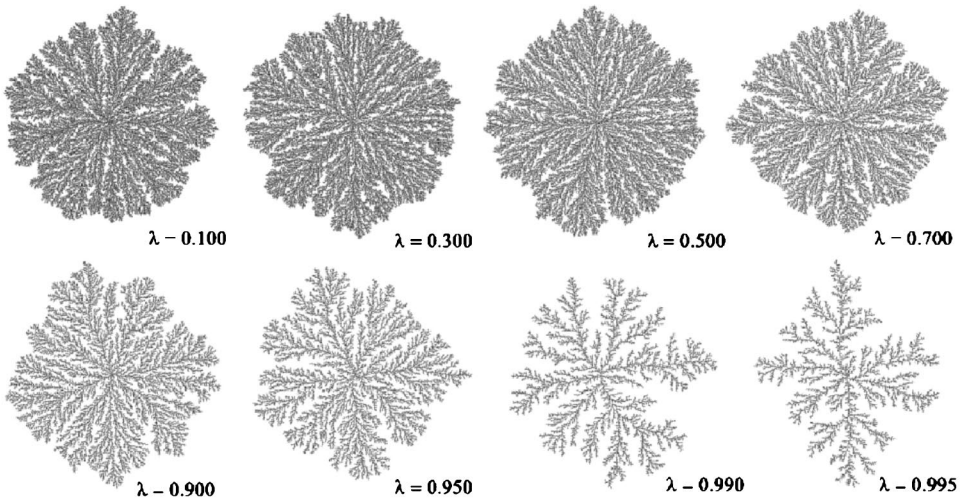

FIG. 4. Morphology transition between BA and DLA growth patterns. The number of aggregated particles varies from 2.5×10^5 ($\lambda=0.1$) to 5×10^4 ($\lambda=0.995$).

conclude that the γ exponent is nonuniversal, i.e., depends on the lattice structure.

In Fig. 5, the double-logarithm plots of $\overline{\rho}-\rho_0$ as a function of r for distinct λ values are shown. The density ρ_0 was obtained by searching for the best linear fit in the larger linear region. To avoid the active region, we limited the fits to those data corresponding to a half of the cluster sizes. Depending on the λ value, lattices with linear size $L=5\times10^3$ or $L=10^4$, and 10–20 independent runs were used. One can observe a power law regime for $r>10$ showing that the approach to the stationary value obeys Eq. (5). In Fig. 6, the asymptotic density ρ_0 and the γ exponent are shown as functions of $1-\lambda$, the distance from the transition point. ρ_0 acts as an order parameter, which vanishes at the critical point following a relation $\rho_0\sim|1-\lambda|^{\beta}$. The exponent obtained from the data of Fig. 6(a) was $\beta=0.27(1)$, whereas the exponents obtained for $L=2\times10^3$ and 10^4 were $\beta=0.28(2)$ and 0.26(1), respectively. The numbers in parentheses represent the uncertainties. In Fig. 6(b), the γ exponents for distinct λ values are shown. One can observe that γ fluctuates around the value 0.46. The smaller value found was $\gamma\approx0.43$ and the larger one $\gamma\approx0.48$. Our simulations suggests that the γ exponent is independent of λ and its value is $\gamma=0.46\pm0.02$. The error indicated in the γ value was evaluated through an average over the data of Fig. 6(b).

In order to test the universality of the γ and β exponents we studied two versions of the present model. In the first one, we use square lattices, but the walkers stick to the cluster if they reach a nearest or a next-nearest empty neighbor of an occupied site. In the second one, we use a hexagonal lattice. Lattices with size $L=2000$ were used. The exponents for the first modified version were $\beta=0.27\pm0.02$ and $\gamma=0.49\pm0.03$, and the exponents for hexagonal lattice were $\beta=0.28\pm0.02$ and $\gamma=0.49\pm0.03$. These results lead us to conclude that these exponents are universal.

The morphological transition between BA and DLA models was also characterized by the crossover radius ξ defined in Eqs. (1) and (2). The number of particles $M(r)$ inside a region delimited by a circle of radius r centered at origin was evaluated. The M vs r curves exhibit tenuous crossovers determining the transition between DLA- and BA-like scaling regimes. In Fig. 7(a), an example of this crossover is shown. Since the growth patterns scale as DLA (BA) for small

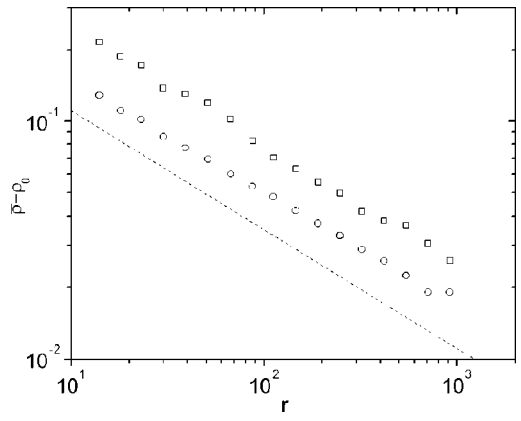

FIG. 5. Double-logarithm plots of $\overline{\rho}-\rho_0$ against r for $\lambda=0.3$ (squares) and 0.99 (circles). The dashed line corresponds to the slope −0.46. The linear fits of the data provide $\gamma\approx0.45$ for $\lambda=0.3$, and $\gamma\approx0.47$ for $\lambda=0.99$.

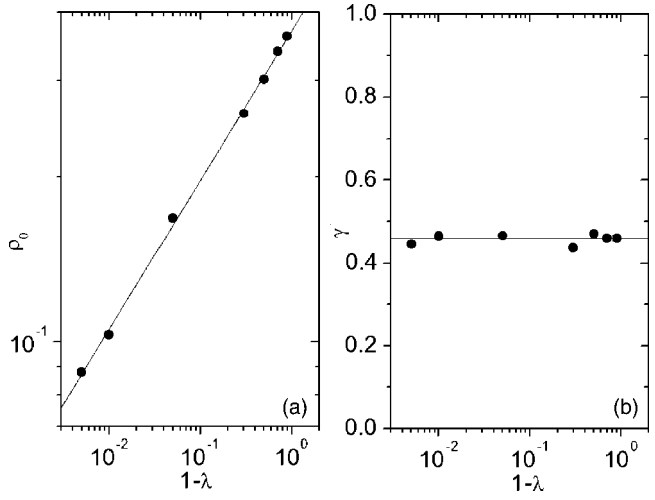

FIG. 6. (a) Stationary density ρ_0 and (b) γ exponent defined in Eq. (5) as a function of the distance from the transition point. The lattice size used was $L=5\times10^3$ and simulation stopped when the cluster reaches the lattice edge.

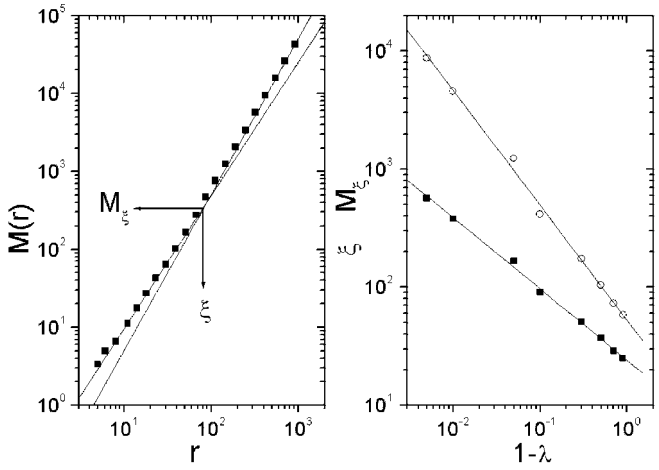

FIG. 7. (a) Determination of the crossover between DLA- and BA-like scaling regimes for $\lambda=0.90$. The straight lines represent the slopes 1.71 and 2, i.e., the fractal dimensions for DLA and BA models, respectively. (b) The crossover length (squares) and the corresponding mass (circles) as a function of the distance from the transition point. These results were obtained for $L=5\times10^3$.

(large) length scales, in order to evaluate the crossover ξ we fitted the curves by power laws $M(r)\sim r^{d_f}$, where $d_f=1.71$ and 2 were used for the initial and the final curve regions, respectively. The crossover lengths obtained through this method are drawn as a function of the distance from the transition point in Fig. 7(b). The length ξ diverges at $\lambda=1$ following a power law $\xi\sim|1-\lambda|^{-\nu}$, where $\nu=0.61(1)$. Moreover, the mass at the critical point diverges as $M_\xi \sim|1-\lambda|^{-\alpha}$, where $\alpha=0.97(2)$.

As discussed in Sec. I, these crossovers between fractal and homogeneous patterns occur due the crossover in the particle trajectories. However, the crossover length of the walker trajectories is given by (see the Appendix)

$$\xi_w=\frac{\pi\lambda}{\sin(\pi\lambda)}-\frac{\sin(\pi\lambda)}{\pi\lambda}, \tag{6}$$

which diverges as $\xi_w\sim|1-\lambda|^{-1}$ for $\lambda\lesssim1$. Thus, although the transition between DLA and BA models is due to the transition in the walk dimensionality, the corresponding crossover lengths are not proportional.

Notice that Eq. (5) describes the mean density behavior when $r\gtrsim\xi$. Moreover, $\overline{\rho}\sim r^{d_f-2}$ when $r\ll\xi$ due to the cluster fractality on this length scale. Thus, using Eq. (5), we found that the mean density at the crossover can be written as

$$\overline{\rho_\xi}=A_1|1-\lambda|^{\beta}+A_2|1-\lambda|^{\nu\gamma}, \tag{7}$$

where A_1 and A_2 are constants. But the mean density at the crossover is given by

$$\overline{\rho_\xi}\sim\frac{M_\xi}{\xi^2}\sim|1-\lambda|^{2\nu-\alpha}. \tag{8}$$

Comparing Eqs. (7) and (8), we have that they are consistent only if

$$\beta=\nu\gamma \quad \text{and} \quad \beta=2\nu-\alpha. \tag{9}$$

In agreement with the scaling relation (9), the number of independent exponents is reduced from 4 to 2. Using the exponents measured for systems with size $L=5000$, we found $\nu\gamma=0.28(2)$ and $2\nu-\alpha=0.25(3)$, in addition to $\beta=0.27(1)$. The difference between these values is inside the error margins indicated in the parentheses. The large uncertainties obtained in the exponents (5%–10%) originate in the difficulty in determination of the exact crossover points.

IV. CONCLUSIONS

In the present work, we studied the transition between diffusion-limited aggregation and ballistic aggregation models. We used a model in which the random walks in the DLA model are replaced by biased random walks with a drift in a random direction. The drift is controlled by a parameter $\lambda\in[0,1]$ that leads the model from BA ($\lambda=0$) to DLA ($\lambda=1$) [see Eq. (3)]. Also, an efficient algorithm, which allows large scaling analysis of the growth patterns, was introduced.

For any bias, the clusters are fractal (DLA-like) on the short length scales whereas nonfractal patterns are obtained on the large ones. The transition between DLA- and BA-like scaling regimes is determined by a characteristic length ξ that diverges as $\lambda\to1$ following a power law $\xi\sim|1-\lambda|^{-\nu}$, where $\nu=0.61(1)$, while the cluster mass at the crossover follows the relation $M_\xi\sim|1-\lambda|^{-\alpha}$, where $\alpha=0.97(2)$. This crossover was not numerically determined in similar previous work. The density in the inner regions of the cluster reaches an asymptotic value $\rho_0\sim|1-\lambda|^{\beta}$, where $\beta=0.26(1)$. However, this approach is slow and follows a power law decay with a universal exponent $\gamma=0.46(2)$ independent of the drift. These exponents obey the scaling relations $\beta=\nu\gamma$ and $\beta=2\nu-\alpha$.

It is worth stressing two main contributions of the present work. The first one is the development of an algorithm that can be used to study other models with biased random walks as for example those related to deposition processes [15,16], for which the determination of universality classes is hard work. The second one is the careful quantitative characterization of the transition between DLA and BA growth models that, in our knowledge, was not previously done. The understanding of these crossovers can be an essential tool in the analysis of real fractals, which always exhibit scaling in limited ranges.

ACKNOWLEDGMENTS

We would like to thank M. L. Martins and A. P. F. Atman for critical reading of the manuscript. This work was partially supported by the CNPq Brazilian agency.

APPENDIX: DEMONSTRATION OF EQ. (6)

For the sake of simplicity, we consider Eq. (3) with a drift direction $\varphi=0$ and $x_0=y_0=0$. Iterating Eq. (3) for n steps, we found

$$\langle x_n \rangle = \sum_{i=1}^{n} \langle \cos(\lambda \theta_i) \rangle \tag{A1}$$

and

$$\langle x_n^2 \rangle = \sum_{i=1}^{n} \sum_{j=1}^{n} \langle \cos(\lambda \theta_i) \cos(\lambda \theta_j) \rangle . \tag{A2}$$

But

$$\langle \cos(\lambda \theta_i) \rangle = \frac{1}{2\pi} \int_{-\pi}^{\pi} \cos(\lambda \theta) d\theta = \frac{\sin(\pi\lambda)}{\pi\lambda} \tag{A3}$$

and

$$\langle \cos(\lambda \theta_i) \cos(\lambda \theta_j) \rangle = \left[\frac{\sin(\pi\lambda)}{\pi\lambda} \right]^2 (1 - \delta_{ij}) + \frac{1}{2} \left[\frac{\sin(2\pi\lambda)}{2\pi\lambda} + 1 \right] \delta_{ij}, \tag{A4}$$

where δ_{ij} is the Kronecker delta function.

Substituting Eqs. (A3) and (A4) in Eqs. (A1) and (A2), respectively, we found

$$\langle x_n \rangle = n \frac{\sin(\pi\lambda)}{\pi\lambda} \tag{A5}$$

and

$$\sigma_x^2(n) = n \left\{ \frac{1}{2} \left[1 + \frac{\sin(2\pi\lambda)}{2\pi\lambda} \right] - \left[\frac{\sin(\pi\lambda)}{\pi\lambda} \right]^2 \right\}, \tag{A6}$$

where $\sigma_x^2(n) = \langle x_n^2 \rangle - \langle x_n \rangle^2$ is the variance of the coordinate x_n. With a similar analysis, we obtained

$$\langle y_n \rangle = 0 \tag{A7}$$

and

$$\sigma_y^2(n) = n \frac{1}{2} \left[1 - \frac{\sin(2\pi\lambda)}{2\pi\lambda} \right]. \tag{A8}$$

Thus, the walk mean displacement $r(n) = \sqrt{\langle x_n \rangle^2 + \langle y_n \rangle^2}$ and the variance $\sigma^2(n) = \sigma_x^2 + \sigma_y^2$ are given by

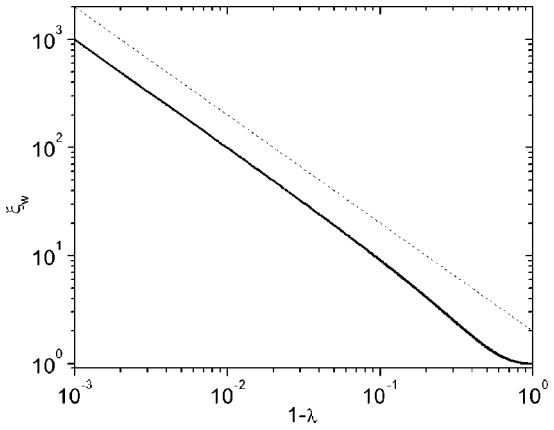

FIG. 8. Double-logarithm plot of the crossover length ξ_w as a function of $1-\lambda$. The solid line represents the data obtained from Eq. (A12) and the dashed line has a slope −1.

$$r(n) = n \frac{\sin(\pi\lambda)}{\pi\lambda} \tag{A9}$$

and

$$\sigma(n) = n^{1/2} \left\{ 1 - \left[\frac{\sin(\pi\lambda)}{\pi\lambda} \right]^2 \right\}^{1/2}. \tag{A10}$$

The crossover of the walk dimensionality ($d=2$ for short times and $d=1$ for long ones) occurs when $r(n) \sim \sigma(n)$. Making equal Eqs. (A9) and (A10), we obtained an estimate of the characteristic number of steps $\mathcal{N}$ necessary for the crossover,

$$\mathcal{N} = \left[\frac{\pi\lambda}{\sin(\pi\lambda)} \right]^2 - 1. \tag{A11}$$

Thus, the characteristic crossover length is

$$\xi_w = r(\mathcal{N}) = \frac{\pi\lambda}{\sin(\pi\lambda)} - \frac{\sin(\pi\lambda)}{\pi\lambda}. \tag{A12}$$

In Fig. 8, ξ_w is plotted as a function of $1-\lambda$. Expanding Eq. (A12) around $\lambda = 1$, we found $\xi_w \sim |1-\lambda|^{-1}$.

[1] P. Meakin, *Fractals, Scaling and Growth far from Equilibrium* (Cambridge University Press, Cambridge, U.K., 1998).
[2] T. Vicsek, *Fractal Growth Phenomena* (World Scientific, Singapore, 1992).
[3] A.-L. Barabasi and H. E. Stanley, *Fractal Concepts on Surface Growth* (Cambridge University Press, Cambridge, UK, 1995).
[4] T. A. Witten and L. M. Sander, Phys. Rev. Lett. **47**, 1400 (1981).
[5] M. Matsushita, M. Sano, Y. Hayakawa, H. Honjo, and Y. Sawada, Phys. Rev. Lett. **53**, 286 (1984).
[6] K. J. Måløy, J. Feder, and T. Jøssang, Phys. Rev. Lett. **55**, 2688 (1985).
[7] M. Matsushita and H. Fujikawa, Physica A **168**, 498 (1990).
[8] F. Caserta, H. E. Stanley, W. D. Eldred, G. Daccord, R. E. Hausman, and J. Nittmann, Phys. Rev. Lett. **64**, 95 (1990).
[9] M. J. Vold, J. Colloid Sci. **18**, 684 (1963).
[10] S. Liang and L. P. Kadanoff, Phys. Rev. A **31**, 2628 (1985).
[11] P. Meakin, Phys. Rev. B **28**, 5221 (1983).
[12] Y. Kim, K. R. Choi, and H. Pak, Phys. Rev. A **45**, 5805 (1992).
[13] Y. Kim and K. R. Choi, Phys. Rev. E **48**, 1586 (1993).
[14] T. Nagatani, Phys. Rev. A **39**, 438 (1989).
[15] M. Castro, R. Cuerno, A. Sánchez, and F. Domínguez-Adame, Phys. Rev. E **62**, 161 (2002).
[16] Y. Kim, J. Korean Phys. Soc. **30**, 511 (1997).
[17] T. Nagatani, Phys. Rev. A **37**, 3514 (1988).
[18] R. C. Ball and R. M. Brady, J. Phys. A **18**, L809 (1985).
[19] P. Meakin, J. Phys. A **18**, L661 (1985).
[20] S. Tolman and P. Meakin, Phys. Rev. A **40**, 428 (1989).
[21] S. C. Ferreira, Jr., Eur. Phys. J. B **42**, 263 (2004).